SQUID-based Systems for Co-registration of Ultra-Low Field Nuclear Magnetic Resonance Images and Magnetoencephalography

Andrei N. Matlashov, Evgeny Burmistrov, Per E. Magnelind, Larry Schultz, Algis V. Urbaitis, Petr L. Volegov, Jacob Yoder, and Michelle A. Espy

Los Alamos National Laboratory, P.O. Box 1663, MS-D454, Los Alamos, NM 87545, USA; e-mail: matlach@lanl.gov

Abstract - **The ability to perform MRI in ultra-low magnetic fields (ULF) of ~100 µT, using superconducting quantum interference device (SQUID) detection, has enabled a new class of magnetoencephalography (MEG) instrumentation capable of recording both anatomical (via the ULF MRI) and functional (biomagnetic) information about the brain. The combined ULF MRI/MEG instrument allows both structural and functional information to be co-registered to a single coordinate system and acquired in a single device. In this paper we discuss the considerations and challenges required to develop a combined ULF MRI/MEG device, including pulse sequence development, magnetic field generation, SQUID operation in an environment of pulsed pre-polarization, and optimization of pick-up coil geometries for MRI in different noise environments. We also discuss the design of a "hybrid" ULF MRI/MEG system under development in our laboratory that uses SQUID pick-up coils separately optimized for MEG and ULF MRI.**

I. INTRODUCTION

Magnetoencephalography (MEG) and magnetic resonance imaging (MRI) were made commercially available approximately at the same time, in the mid 1980s, and have coexisted for more than three decades as two technically incompatible methods. While MEG pushed toward measurements at the femto-Tesla level, MRI was pushing toward operating in magnetic fields some 15 orders of magnitude higher, at the Tesla range. Both methods, however, depended significantly on technical advances in superconductivity. Basically, MEG was born as a consequence of the invention of the SQUID – the superconducting quantum interference device. MRI became a mature and widespread method after the development of high uniformity Tesla-range superconducting magnets. Both methods played crucial roles in research and diagnostics of the brain over the last three decades. However, until recently they were used separately

because of the disparity in magnetic field strengths. MRI provided morphological images of the brain and MEG provided functional images related to bioelectrical brain activity. Both images could be superimposed with each other. However, practically achieving adequate co-registration has often proven challenging.

The idea of making one machine for both MEG and MRI appeared impossible until two key ideas crossed paths. The first idea came from a paper published by Macovsky and Connolly in 1993 that pointed out that the field-cycling pre-polarization technique enables the development of inexpensive low-field MRI machines [1]. The second idea came from advances in SQUID instrumentation. A few groups experimented with SQUIDs for the measurement of NMR signals at low Larmor frequency, usually a few kHz. This technique was pioneered and significantly developed by John Clarke and his colleagues at Berkeley [2]. They recorded the first ever MR images of plants and a human forearm and fingers at 132 µT field [3], which corresponds to a 5.6 kHz Larmor frequency. Such achievements in SQUID-based MRI gained the interest of many MEG groups over the world. The idea of using SQUID arrays for simultaneous detection of both MEG and brain MRI, which could reasonably improve the superposition of images from the two different modalities, and eliminate the requirement for two costly devices, is extremely attractive.

The first proof-of-principle results in recording simultaneous MEG and MRI signals were achieved in 2004 [4], [5]. In this work, the somatosensory evoked magnetic response from the human brain was recorded truly simultaneously with the free induction decay (FID) signal at 268 Hz. During such experiments it became clear that simultaneous recording of such signals is very difficult to perform because of the large low frequency noise arising from the external magnetic field needed for the NMR precession. This noise was caused by micro-vibrations of the SQUID gradiometer in the NMR field and it seriously distorted the MEG signal. In later experiments MEG and MRI signals were recorded sequentially and the external field and gradients were zeroed during the MEG recording.

The first ever ultra-low field (ULF) MR images of the human brain were published in 2008 [6]. MRIs were recorded by a flat array of 7 axial second-order gradiometers at 46 µT measurement field using liquid nitrogen cooled pre-polarization coils which generated a ~30 mT field. The image resolution was 3 x 3 x 6 mm^3 and the time for one scan was about 15 minutes. Six scans were averaged to improve the signal-to-noise ratio (SNR) of the images up to about 30. Auditory evoked magnetic field signals were recorded immediately after the ULF MRI session was finished. However the subject moved slightly for better coverage of the MEG signals, which prevented co-registration. These results demonstrated that one SQUID-based system could be used for both ULF MRI of the human brain and MEG.

Although it was almost impossible to record true simultaneous MRI and MEG signals of high quality, it was possible to record interleaved signals during one session. Such co-registration of auditory evoked magnetic field mapping and ULF MR imaging was performed in 2010 [7]. This time the MEG map was accurately superposed with the MR Images. The co-registration error of the different coordinate systems was within 1 mm accuracy.

This paper describes our group's experience in the development of SQUID-based instruments for combined ULF MRI and MEG measurements. We also provide some

estimations and views regarding potential performance and development of such systems, and discuss a system we are in the process of developing.

II.   ULF MRI – MEG SYSTEM GENERAL DESIGN

A combined MEG and ULF MRI system is not just an upgraded conventional MEG machine. Adding ULF MRI capability implies the addition of coils for generation of fields and gradients. In principle this could be viewed as some sort of simple upgrade. However, in addition to the MRI coils there are completely new requirements on the SQUID-based sensors. One of the most difficult requirements is that the SQUIDs should work immediately after being exposed to a pre-polarizing field of up to 0.2 T.

The second difference between MEG and MRI systems is that the optimization criteria for the pick-up coil sizes are quite different. For MEG the pick-up coil diameter should be small enough to avoid smoothing of spatially sharp field distributions [8]. Commonly used pick-up coil diameters in MEG systems are in the range 5–20 mm. In the case of ULF MRI the spatial resolution is defined by the applied gradients and the voxel SNR but not by the pick-up coil diameter. This is why ULF MRI systems may need a lesser number of pick-up coils of larger size to cover the same area of interest. One approach is a hybrid design with different size and quantity of pick-up coils for recording of MEG and MRI signals.

We will now describe the main components of such a system. We limit this discussion to systems used inside a magnetically shielded room (MSR) typically used for biomagnetic measurements [9]. A combined MEG and ULF MRI system consists of the following main components: 1) a SQUID magnetometer or gradiometer array for MEG and ULF MRI which may include the same sensors for both, or have sensors individually optimized for each, 2) a pre-polarizing field coil system, 3) a measurement field coil system, 4) a group of coils to generate gradients needed for MR imaging, and 5) possibly spin-flip coils. All SQUID sensors are placed inside a liquid helium fiberglass cryostat in such a way that the subject's head can be placed in close proximity to all the pick-up coils. The coil systems for generation of small magnetic fields and gradients required for imaging can be made large enough to accommodate the subject placed in a chair or on a bed. It is one advantage of the ULF MRI technique that these fields do not have to be highly homogeneous. The pre-polarizing coil system should be placed as close to the volume of interest as possible in order to maximize the field. It can be designed either as resistive coils with a cooling system or as a superconductive coil placed inside the cryostat with the SQUIDs [10] or inside a separate cryostat. In the following sections we will discuss these components in detail.

III.   PULSE SEQUENCES

A. Standard Pulse Sequences for ULF MRI

The relatively small magnetic fields that are used in ULF MRI enable versatile and unique pulse sequences. This is because the requirements on the hardware to produce and manipulate these fields are relaxed compared to high field MRI. A standard pulse sequence for ULF MRI consists of 1) pre-polarization, 2) inducing precession, 3) spatially encoding the spins, 4) creating an echo, and 5) read out of the signal echo or echoes.

Two typical pulse sequences for ULF MRI are shown in **Error! Reference source not found.**. We will now describe the different parts of the pulse sequence individually.

Pre-polarization. The pre-polarizing field technique is widely used for field-cycling NMR relaxometers since its first introduction in 1954 [11]. In 1993 this technique was proposed for low-cost medical MRI instruments [1]. It is based on a simple idea of pre-polarizing a sample at a large and not very uniform field, which is switched off and a more uniform low measurement field is applied to produce the proton spin precession.

A feature of the field-cycling technique is that it is possible to have an intermediate relaxation field, in which the spins relax after the pre-polarization. This enables investigations of dispersion of the T_1 contrast at any field between the pre-polarization and the readout fields.

Initiation of spin precession. If the pre-polarizing field is switched off very quickly or non-adiabatically ($dB_p/dt \gg \gamma B_m^2$) the proton spins stay oriented along their initial direction and they will start precession around a small measurement field that is applied in an orthogonal direction. This simple method has a few disadvantages. First, it requires a very fast switching-off process (which is technically challenging to achieve) and also the large dB/dt may generate large eddy currents or transients in surrounding conducting parts. Second, the initial spatial orientation of the proton spins is not the same because it depends on the local directions of the non-uniform pre-polarizing field. Hence, the spins start precession with different initial phases.

If the pre-polarizing field is switched off adiabatically, the proton spins become oriented along the smaller and much more uniform measurement field. In this case a spin-flip magnetic pulse should be applied at the Larmor frequency and orthogonally to the measurement field to turn the proton spins in an orthogonal direction to the measurement field to start their precession. Such a technique requires additional spin-flip coils and a spin-flip $\pi/2$ pulse with specific shape, frequency and amplitude.

Spatially encode the spins. To create the final image, the spins need to be spatially encoded by frequency and/or phase. This is achieved by applying encoding gradients for some time after initiating the precession and the free induction decay (FID) has started. The encoding gradients shift the phase, and/or the frequency of the spins depending on the spatial location. The resolution of the image depends on the applied gradients, as will be discussed later. A feature of the field-cycling technique is that it is possible to have an intermediate relaxation field, in which the spins relax after the pre-polarization. This enables investigations of dispersion of the T_1 contrast at any field between the pre-polarization and the readout fields.
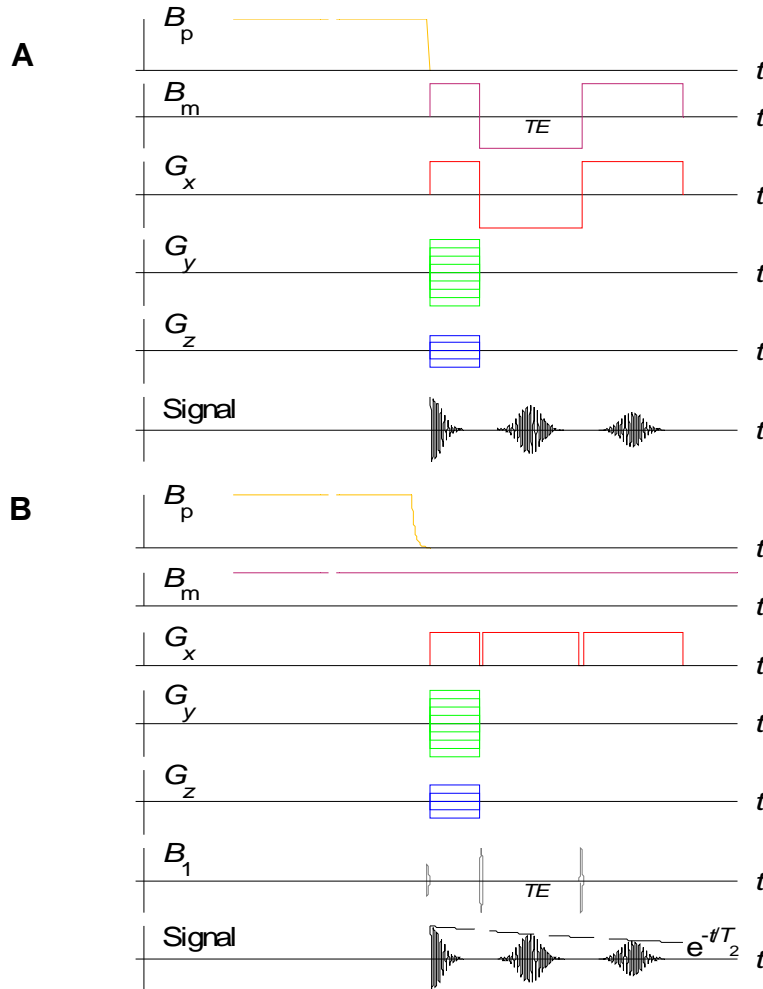
Fig. 1. Pulse-sequences for gradient-echo (A) and spin-echo (B) ULF MRI with two echoes. The gradient-echo is shown with a non-adiabatic ramp-down of B_p and subsequently the measurement field, B_m, is turned on in an orthogonal direction. The echo is created by changing the polarity of both the frequency-encoding gradient and the measurement field. At the echo-time, TE, the echo has a maximum. In the spin-echo sequence, the B_p field is ramped down adiabatically and the precession is started by a $\pi/2$ pulse. After half the echo-time a π pulse is applied to form the echo, which is centered at TE. The amplitude of the echo is given by the transverse relaxation time, T_2, as indicated by the dashed line.

Create an echo. After the encoding period most MRI sequences rely on the use of an echo to remove the effects of dephasing due to magnetic field inhomogeneities. There are two different ways to achieve the echo. First, the polarity of the frequency-encoding gradient can be changed and at ULF one can also change the polarity of the measurement field, B_m. Alternately, a π pulse can be applied to flip the spins.

A rephasing process begins and the signal reaches a maximum at TE, which is the time of the spin-echo. The amplitude of the spin-echo is given by the transverse relaxation time T_2, which is independent of static magnetic field inhomogeneities.

B. Other Pulse Sequences

High-field systems are routinely used for numerous different applications in medical imaging. There are many examples of pulse sequences optimized for specific imaging tasks at high field, and several of these sequences can be leveraged for ULF MRI applications as well. However, ULF MRI also has unique capabilities (e.g. the ability to easily reorient the measurement field, or change the Larmor frequency) and considerations (e.g. shortening of T_1 with reduction in field strength). Recently a few such applications have been explored at ULF.

Functional MRI at ULF requires a different approach than at high field, where the Blood Oxygen-Level Dependent (BOLD) response is the most commonly used. The reason is that BOLD relies on the susceptibility difference between oxy- and deoxy-hemoglobin, i.e. oxygenated and de-oxygenated blood. Since the susceptibility effect scales with the measurement field, it is negligible at ULF. Hence, flow-based imaging techniques have to be used instead. We have recently presented preliminary phantom data of an arterial spin-labeling approach called FAIR (Flow-sensitive Alternating Inversion Recovery) [12] at ULF [13]. FAIR is a method in which two images (tag and control) are subtracted from each other to generate a flow image. An adiabatic inversion pulse is applied with and without a slice-select gradient present to create the tagged and control images, respectively. A potential advantage of hemodynamic functional imaging at ULF is the ability to combine it with MEG, which could provide additional insight into the relationship between the hemodynamic and biomagnetic response of the brain to neurological function. However, a challenge is that T_1 times are shortened (from ~ 1 s at 1.5 T to ~ 0.2 s at 100 μT) which restricts the signal available if long flow times are required. Thus, it might be necessary to let the spins relax in the pre-polarizing field instead of the measurement field.

We have also recently demonstrated preliminary measurements of Magnetic Resonance Electrical Impedance Tomography (MR-EIT) [14] in a phantom at ULF [13]. A static current is passed through electrodes and the induced magnetic field adds to the measurement field and creates a detectable phase-shift of the MR signal. MR-EIT has been of interest in conventional high field MRI because of the potential to extract new contrast via impedance changes in tissue (for example stroke or changes between benign and cancerous tissue). There may be additional advantages to performing MR-EIT in the ULF (kHz) regime, where tissue contrast is optimized and off-axis components of the induced magnetic field may be obtained by overlapping the frequency of the applied current with the Larmor frequency.

Since most of the scan time in ULF MRI is spent on pre-polarization, it is appealing to use consecutive echoes to cover different points in *k*-space. In Echo Planar Imaging (EPI) [15] this is achieved by a multi-echo sequence with the read-out gradient switching polarity as in a regular gradient-echo sequence. However, each gradient-echo is individually phase-encoded. Because small errors can build up over echoes, greater accuracy in phase encoding is required. EPI has not yet been demonstrated at ULF.

Recently, Nieminen et al. [16] described an interesting pulse sequence, in which the pre-polarization is used to encode the spatial locations. The technique, which they call polarization encoding, would provide faster imaging, as the encoding period is removed and one would only use the FID signal. Hence, there is no need for an echo.

IV.   OPTIMIZATION OF THE PICK-UP COIL SIZE FOR MRI

The spatial resolution of MR imaging is defined by the maximum encoding gradients and the encoding time:

$$\Delta l \approx 1 / (2\gamma T_{ENC} \cdot G_{MAX}), \qquad (1)$$

where G_{MAX} is the maximum encoding gradient, T_{ENC} is the encoding time, and γ is the proton gyromagnetic ratio (42.58 MHz/T). This equation is applicable if there is adequate signal amplitude at the maximum encoding gradients; in particular, the voxel SNR should be significantly higher than 1.

The magnetic flux produced by a small volume of material (voxel) through a pick-up loop is proportional to the magnetic moment of the voxel and also depends on the geometrical coupling. The magnetic moment of a voxel is proportional to its volume and the pre-polarizing field. The geometrical coupling depends on the voxel position and the pick-up coil size. The magnetic flux generated by a voxel is transformed from the pick-up loop into the SQUID loop via a superconducting flux transformer. To estimate the signal from a single voxel we need to know its magnetic moment and calculate the portion of its flux that reaches the SQUID loop. The SQUID loop flux depends on the pick-up coil diameter, which can be optimized, and the SQUID sensor parameters. Theoretically, SQUID sensor parameters can also be optimized but in practice it is an intricate process. Therefore, we avoid this part of the optimization process and limit our discussion to the commercial SQUID sensor, the CE2Blue from Supracon [17]. We have routinely used this SQUID model in our systems because it is the only commercial sensor available with an embedded cryogenic switch at this time.

In the numerical optimization we follow the approach outlined in Ref. [18]. We begin by numerically solving the Bloch equation for a single magnetic moment. We then average it to get the magnetization of a 1 mm^3 water voxel. By using the reciprocity principle we recalculate the magnetic flux inside of a pickup loop. Thereby we calculate the maximum amplitude of the magnetic field from every water voxel detected by the pickup coil. In other words we calculate the NMR signal of every water voxel detected by pickup coil at the very beginning of the free induction decay. In our optimization we assume a 200 mT uniform pre-polarization field.

For optimization of the pick-up coil diameter and estimation of the single voxel SNR at different voxel positions we used the CE2Blue's parameters: L_{IN} = 420 nH input coil inductance and 0.26 µA/Φ_0 input current sensitivity. A pick-up coil with a diameter varying from 5 to 100 mm is connected to the SQUID sensor assuming a 10 cm long twisted pair (100 nH). **Error! Reference source not found.**A shows the magnetic flux in the SQUID as a function of the distance from a single 1 mm^3 water voxel for different pick-up coil diameters. **Error! Reference source not found.**B shows how the magnetic flux in the SQUID depends on the pick-up coil diameter for different distances to the voxel. For shallow locations with depth less than 25 mm the optimal pick-up coil diameter is between 40 and 65 mm. For deeper locations the diameter should be larger than 65 mm. In both cases the optimal coil diameter for MRI is much bigger than what is considered to be optimal for MEG signal detection.
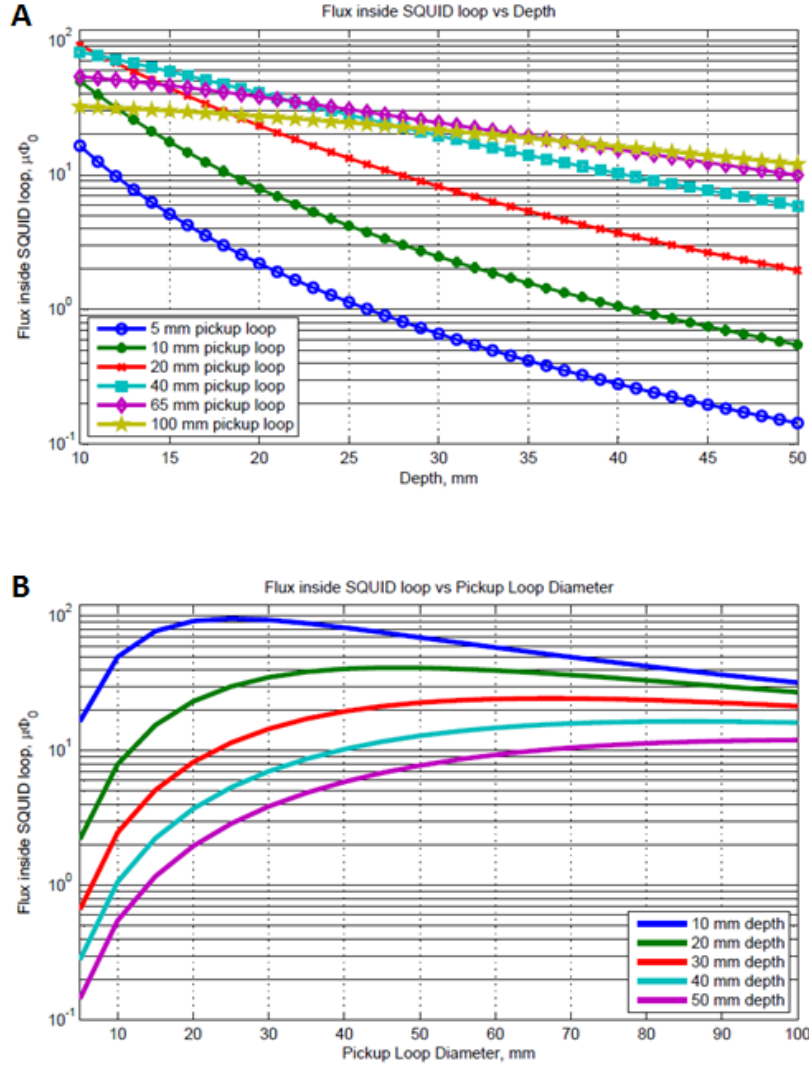
Fig. 2. Calculated flux inside the SQUID loop versus 1 mm³ voxel depth for different diameter pick-up loops (A) and versus pick-up loop diameter for different depths (B). For shallow depths (<25 mm) a 45-65 mm diameter coil is preferred, while for greater depths a larger coil provides greater signal.

Our calculations can also be used for estimations of voxel SNR. We may assume that the total system noise is defined by a SQUID intrinsic noise equal to 3 $\mu\Phi_0/\sqrt{Hz}$, which corresponds to about 0.42 fT√Hz input field noise with a 40 mm diameter pick-up coil. In this case the SNR at unity bandwidth decreases from 25 to 2 as depth increases from 10 to 50 mm. This SNR uses the maximum voxel magnetization (neglecting relaxation) at 0.2 T field. To calculate the voxel SNR detected using a particular pulse sequence we need to add corrections associated with the MRI pulse sequence. Following the analysis of voxel SNR for MRI described in Ref. [19] and using equation 2.40:

$$ SNR_{voxel} = \frac{\mu_0 \beta_\perp}{4\pi A_p S_B^{1/2}} M_{echo} V_{voxel} \sqrt{\frac{N_{av} N_y N_z T_s}{2}}, \qquad (2) $$

where N_{av} is the number of averages for each acquisition step, N_y is the number of encoding steps in the y direction, N_z is the number of encoding steps in the z direction, T_s is the data acquisition time, V_{voxel} is the voxel volume, M_{echo} is the magnetization at the echo time, μ_0 is the permeability of vacuum, $\beta\perp$ is the part of the reciprocal field produced per unit current flowing through the pick-up loop at the voxel ($\mu_0\beta(\mathbf{r})/4\pi$) which is perpendicular to B_m, A_p is the pick-up coil area, and $S_B^{1/2}$ is the equivalent magnetic field sensor noise; we estimated voxel SNRs using the following settings: $N_{av} = N_z = 1$, $N_y = 63$, $T_s = 205$ ms. The magnetization M_{echo} was estimated for water using equation 2.48 and the pulse sequence shown on Fig. 2.12 in Ref. [19]. A 40 mm pick-up coil will have an SNR of 146 for a $2\times2\times5$ mm^3 voxel placed at 25 mm depth and 32 at 50 mm depth.

We considered an ideal case when the system noise comes only from the SQUID sensor. In practice the total noise of an ULF MRI system may be caused by a complex combination of different noise sources such as Johnson (thermal) noise from the cryostat or the radio-frequency interference (RFI) shield, or noise coming from field generating electronics. Based on our experience we may conclude that the total field noise referred to a pick-up coil is usually about 1 fT/$\sqrt{}$Hz. It probably can be decreased down to 0.3 fT/$\sqrt{}$Hz by further improvement of system components; however our experience indicates that it would be challenging to achieve 0.1 fT/$\sqrt{}$Hz. To understand the influence of 1 fT/$\sqrt{}$Hz background noise on the efficiency of the detection system we performed a simple numerical experiment.

Based on our calculations of magnetic flux from every water voxel we recalculated the the voxel SNR of three different pickup coil systems in two scenarios: 1) only SQUID noise is present in the system, and 2) a 1 fT/$\sqrt{}$Hz background noise is present in addition to the SQUID noise. The first pickup coil system consists of one 40 mm pickup coil, the second system is 60 mm pickup coil and the third one is the system with seven 20 mm pickup coils. At first it is interesting to compare one 60 mm pickup coil with seven 20 mm 20 mm ones, because both systems cover approximately the same area (inset of

Fig. 3). In the case of only SQUID noise the results are intuitive, the 60 mm pickup coil has a much better SNR because the aggregate noise of seven 20 mm magnetometers is increased by a factor of $\sqrt{7}$. The situation changes dramatically with a 1 fT/$\sqrt{}$Hz background noise level not correlated in neighbor channels, such as thermal noise from superinsulation or RFI shield (

Fig. 3). The 60 mm pickup coil gives an additional 14.4 $\mu\Phi_0/\sqrt{}$Hz to the SQUID's intrinsic 3 $\mu\Phi_0/\sqrt{}$Hz noise inside the SQUID loop, whereas a single 20 mm pickup coil gives only 2.0 $\mu\Phi_0/\sqrt{}$Hz in addition. Hence, a system with seven 20 mm pickup coils is preferable to a single 60 mm pickup coil in this scenario. This result can be easily explained -- small magnetometers average both internal and external noise (if the noise is not correlated in the channels) that leads to $\sqrt{N}$-fold improvement of SNR from distant voxels. In

Fig. 3 we also present the SNR from a 40 mm pickup coil for both noise scenarios. In case of 1 fT/$\sqrt{}$Hz background noise the 40 mm pick-up coil gives approximately 3 times higher 1 mm^3 voxel SNR than the 60 mm one and presents a compromise that provides reasonable sensitivity to both shallow and deeper sources.

When we considered the design of our own new system for co-registered MEG and ULF MRI we assumed the background noise would not be much less than 1 fT/√Hz. Therefore we conclude that 40 mm is the preferred diameter for the MRI pickup coil. It is sensitive to deep objects and still enough sensitive to sources at the surface of a subject's brain (see Error! Reference source not found.**). It is substantially larger than standard MEG pickup coils, but still small enough to not be too sensitive to a 1 fT/√Hz background noise (see**

Fig. 3). The 40 mm diameter pickup coil gives 7.1 $\mu\Phi_0$/√Hz flux noise from the 1 fT/√Hz background noise in addition to the SQUID's intrinsic 3 $\mu\Phi_0$/√Hz inside the SQUID loop.
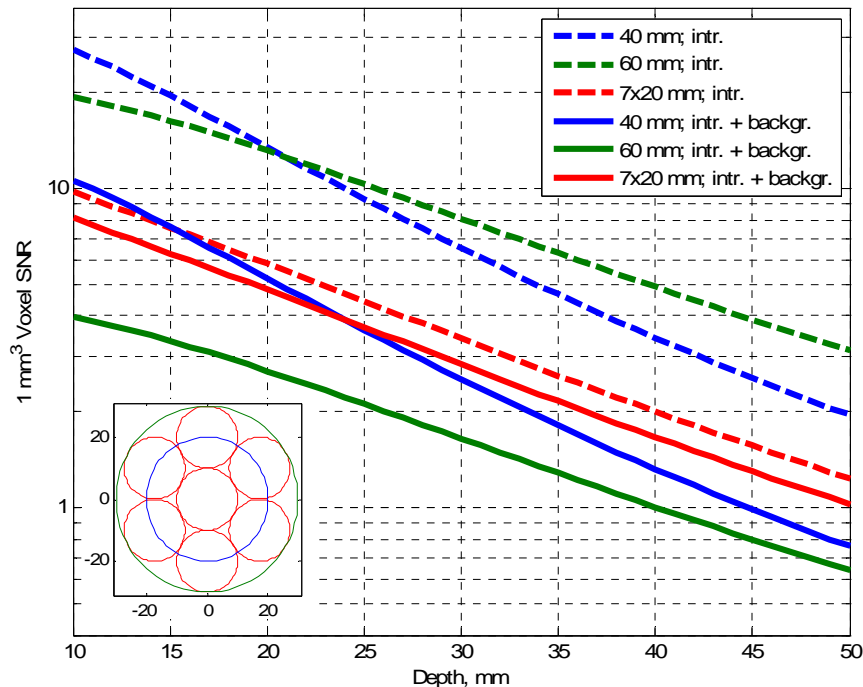

Fig. 3. Signal-to-noise ratio from a 1 mm^3 voxel for three different pickup loop configurations: (blue) a single 40 mm pickup loop, (green) a single 60 mm pickup loop, and (red) seven 20 mm pickup loops. The dashed lines correspond to the situation with only intrinsic SQUID noise (3 $\mu\Phi_0$/√Hz) in the system. The solid lines correspond to a 1 fT/√Hz background noise in addition to the SQUID's intrinsic noise. The inset shows the layout of pick-up coils used in the simulations: (green) a 60 mm diameter coil, (blue) a 40 mm diameter coil, and (red) seven 20 mm diameter coils.

# V.   HARDWARE FOR FIELD GENERATION

A. Pre-polarizing Field

In this section we now discuss some of the more practical aspects of magnetic field generation for ultra-low field MRI.

In both non-adiabatic and adiabatic cases the switching off process is still fast enough to generate transient currents in conducting surfaces such as magnetically shielded room

walls and other conducting parts present around and in the system. Such transient currents can be long relative to T_2 such that signal is lost while waiting for them to decay, and large enough to result in saturation of the SQUID electronics. The pre-polarizing pulses may also magnetize the walls of the MSR and produce increasing wall magnetization and field drift inside the MSR that will distort imaging gradients and shift the Larmor frequency. One possible solution to this problem is using a compensation coil that produces transient currents in the MSR in opposite direction to currents generated by the pre-polarizing pulses [10]. Such a compensation coil should be much larger than the pre-polarizing coil and be oriented in opposite direction to compensate at some level the pre-polarizing field. This method suppresses transients and decreases walls magnetization, but it requires an additional large coil.

Large switching transient pulses may produce trapped fluxes in a SQUID sensor and its components. To avoid this problem two techniques have been used. The first one is based on the "flux dam" idea [20] and the second uses cryogenic superconducting switches [17]. Flux dams work very quickly but usually do not allow outside timing control and also cannot zero current in the flux transformers. Cryogenic superconducting switches have an on-off time of about 5 μs and provide the luxury of a simple external control plus they ideally zero the flux transformer current, but they also increase the liquid helium boil-off rate.

In our instruments we have used the following approach. The transient pulses received by the SQUID sensors have an exponential decay shape that has high frequency spectrum content in the beginning but that moves to lower frequencies at later times. We designed a second electronic feedback that is frequency dependent. This feedback makes the sensors much less sensitive at lower frequencies and the dynamic range for low frequency signals is increased. Fig. 4A shows the schematic of such a second feedback. The schematic parts inside the dashed lines illustrate a conventional feedback loop SQUID electronics that provides, e.g., 1 V/nT sensitivity, where 1 Volt of output signal corresponds to 1 nT input field over the whole frequency range. This output is connected to the second feedback that includes an integrator and an n-fold stronger feedback driver. Fig. 4B shows how the system sensitivity becomes frequency dependent when the second feedback is on. The output signal will be $1/n$ Volt for a 1 nT signal with only low-frequency content and it increases to the normal 1 V/nT at frequencies above $F_{\text{CUT-OFF}}$, which depends on the RC value of the integrator [21], [22].
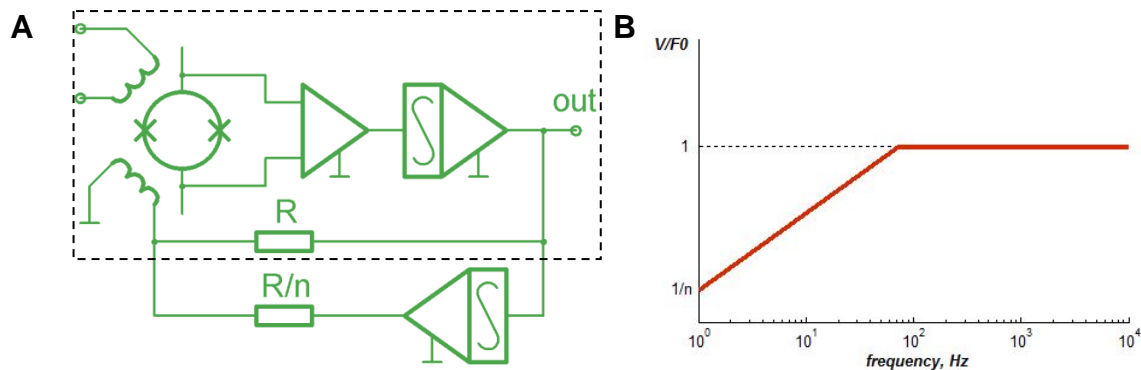
To illustrate the efficiency of this method we describe here one particular application. We used $n = 10$ and $F_{CUT-OFF} = 2$ kHz with a 4 kHz MRI central Larmor frequency. The donut shaped pre-polarizing coil had the following dimensions: $OD = 660$ mm, $ID = 430$ mm and $H = 100$ mm and an inductance of 0.2 H. The coil generated a 100 mT field in its center. The pre-polarizing system was placed inside the MSR size H 3.0 x D 3.7 x W 3,0 m^3 with 25 mm outer aluminum walls and 6 mm inner mu-metal layers. The 7-channel SQUID system was placed 300 mm above the pre-polarizing coil aligned along its axis. It consisted of the 7 axial second order gradiometers 90 mm diameter and 90 mm baseline. The method above decreased the required dead-time after-pulsing due to

Fig. 4. (A) Second feedback circuit schematic showing the regular feedback circuit within the dashed box and the added second feedback with the integrator and a R/n resistor for n-fold deeper feedback. (B) Frequency response of the second feedback loop showing reduced sensitivity at low frequencies.

transients from more than 1 s down to about 10 ms. This system was successfully tested as a ULF MRI scanner for the abdominal area and the knees of a healthy human subject [23].

The second problem associated with the pre-polarizing pulses may be significantly suppressed by using a short, 0.1 s, negative pre-pulse before the main 1-2 s long pre-polarizing pulse is applied. This negative pulse magnetizes the MSR walls in opposite direction with respect to the following longer pulse. It keeps the starting point of the mu-metal hysteresis curve always the same, which suppresses the buildup of magnetization of the walls and field drifts inside the MSR.

B. Measurement Field and Gradient Coils for ULF-MRI

As in conventional MRI, there are many competing requirements for the design of the measurement field and gradient coils: high uniformity, compactness, low power consumption, low inductance and patient accessibility are all important. Some requirements, such as uniformity for the measurement field, are relaxed in the ULF regime since T_2^* depends on absolute, not relative, gradients. There are also subtle requirements that guide the design of the coils, bobbins and hardware. For example, the need to reduce Johnson noise leads one to avoid use of large metal surfaces in the bobbins.

We employed rectangular coil shapes rather than circular because these can be built to very large size with plastic materials (large circular coils can be made using aluminum channel stock bent into a circle). Fig. 5A shows the coil design currently being constructed; The measurement field, B_m, is provided by a four coil arrangement, with smaller coils on the outside, B_{zz} is produced by a simple pair and B_{zx} is provided by four coils which are transverse to the measurement field (B_{zy} is identical to B_{zx}, but rotated 90° about the z axis). Table I shows the characteristics of these coils, as designed. Field uniformities were calculated over a 30 cm diameter spherical volume. By way of comparison, a team at Harvard recently built [24] a slightly larger set of coils mounted on two circular pieces of aluminum; the maximum deviation observed for these coils was 350 ppm after shimming. Without shimming the LANL B_m coils are expected to have a

maximum deviation of 560 ppm. The Harvard planar B_{zx} coils achieved better uniformity by about a factor of 2, but at the expense of limiting access to the sides of the patient.
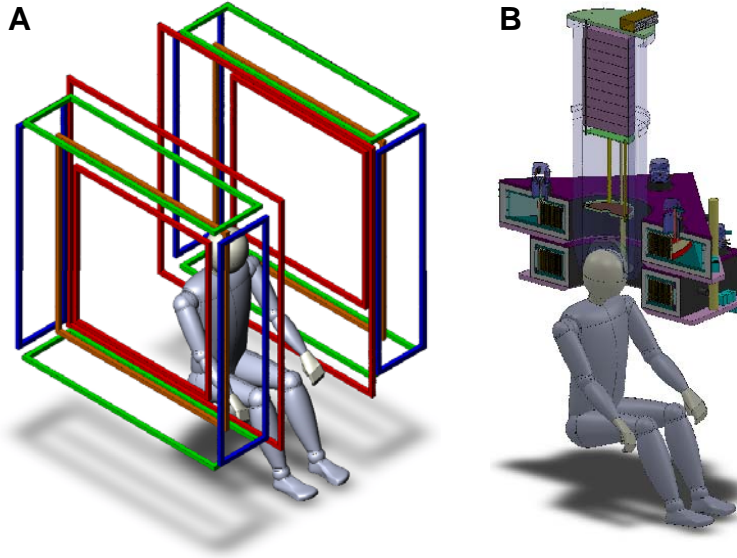

Fig. 5. A) Design of coil assembly for measurement field and gradients. B_m coils (red), B_{zx} coils (blue), B_{zy} coils (green) and B_{zz} coils (orange). B_{zz} coils are coplanar with the smaller, outer B_m coils. B) View of the cryostat and the B_p coils.

Table I. Characteristics of our designed coils; z and x separations refer to distance between centers of coil pairs. Inductance and field characteristics are calculated for coil sets (4 B_m coils, 2 B_{zz} coils, 4 B_{zx} coils).

	z-Sep. (mm)	x-Sep. (mm)	length (mm)	width (mm)	turns per coil	Induct. (mH)	B/I (μT/A) or G/I (μT/m/A)	Max. Dev. (ppm)	RMS Dev. (ppm)
$B_{m,main}$	672	NA	1563	1563	83	109	114	560	130
$B_{m,aux}$	1160	NA	977	977	19				
B_{zz}	1160	NA	1237	1237	24	6	42	25000	4300
B_{zx}	1160	1491	1392	331	66	47	36	20000	6000

VI.   THE NEW LANL SYSTEM DESIGN – MEG AND MRI HYBRID

The sensor system for our new MEG/ULF MRI system will be housed in a Neuromag 122 cryostat that has been completely refurbished to include sensors for both MEG and ULF MRI. The size of the whole system is defined by the size of the measurement coils, which comprise a cube with 1.3 m sides (see Fig. 5). The required volume for the whole system is small enough to fit inside of a standard MEG magnetically shielded room. During a measurement the human subject is sitting between the left and right coil-assemblies. Two pre-polarization coils surround the subject's head as shown in Fig. 5B. The different detectors are located in the Neuromag-122 liquid helium Dewar as shown

in Figure 7. The bottom side of the Dewar fits into the inner diameter of pre-polarization coils.

The results in Refs. [6] and [7] demonstrate the feasibility and potential of human brain imaging with ULF MRI and MEG, but in order to provide the required spatial and temporal resolution of neural activity for clinical relevance it is necessary to increase significantly the number of MRI and MEG channels in the system. Also the optimization criteria for MEG and MRI pick-up coil sizes are quite different and in our new system the detectors for MEG and MRI are separated from each other. For the MEG detection we follow the ideas described in [25] and use square 8x8 mm^2 SQUID magnetometers. For the MRI detection we use Supracon's CE2Blue type SQUIDs with 40 mm circular Nb wire-wound pickup coils as detailed above. The resultant design is shown in Fig. 6.

The whole helmet is divided into 61 clusters where every cluster has one MRI pickup coil (red colored in Fig. 6) and four SQUID magnetometers for MEG detection (blue colored in Fig. 6). Initially we are focusing on an imaging system for the occipital region of the head using only 16 clusters, hence, 16 MRI and 64 MEG channels. At a later stage we will assemble an imaging system for the whole brain with 61 MRI and 244 MEG channels.
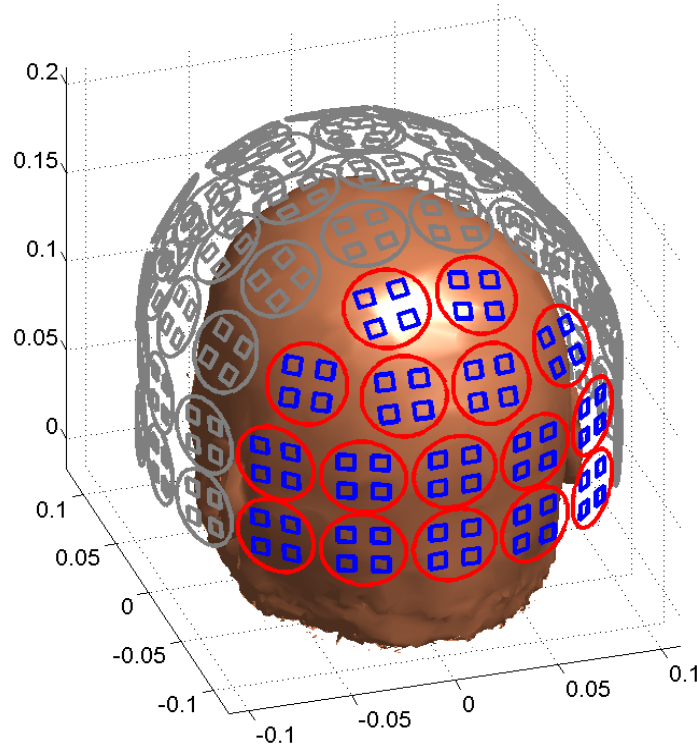

Fig. 6. Helmet shaped whole head array, red circles represent 40 mm pickup coils for MRI detection, blue rectangles represent pickup coils for MEG detection. The structures in gray show the planned future population of the whole array.

VII.   SUMMARY

Solving the ill-posed inverse problem of MEG typically requires co-registration with an anatomical image from high field MRI, imposing both a data co-registration problem and

the requirement for two costly pieces of instrumentation. One of the apparent strengths of the ULF MRI approach is that it naturally allows, for the first time, the combination of MEG and MRI in a single device. There may also be other advantages to ULF MRI in terms of flexible field generation and contrast, and these remain to be fully explored. However, the loss of SNR due to lower magnetization is a serious problem in ULF MRI. The sensitivity of SQUID sensors and use of the highest achievable pre-polarization are techniques to improve this situation, but they impose additional challenges, specifically keeping the SQUIDs operational in this environment and reducing the effects of transient magnetic fields as much as possible. While preliminary demonstrations have shown the feasibility of ULF MRI combined with MEG, thus far these demonstrations have not shown adequate sensor coverage for MEG or SNR for the MRI. Our group and other researchers are now working towards a practical and clinically relevant demonstration of combined MEG and ULF MRI. In this paper we present some of the design considerations, and progress toward such a system.

ULF MRI will always have low SNR compared to conventional MRI, however in certain applications such as combined MEG/MRI it is presently the only solution to a single instrument device. If a clinically acceptable demonstration can be made, and the technical problems are shown to be tractable, it could benefit MEG. It is also possible that a successful outcome here will also advance ULF MRI itself for imaging applications based on unique contrast alone.

ACKNOWLEDGEMENTS

REFERENCES

[1] A Macovski and S. Conolly, "Novel approaches to low-cost MRI," *Magn. Reson. Med.*, **30**, 221–230 (1993).

[2] R. McDermott et al., "Liquid State NMR and Scalar Couplings in Microtesla Magnetic Fields," *Science*, **295**, 2247-2249 (2002).

[3] M. Mössle et al., "SQUID-Detected in Vivo MRI at Microtesla Magnetic Fields," *IEEE Trans. Appl. Supercond.*, **15**, 757-760 (2005).

[4] A. N. Matlachov et al., "Instrumentation for simultaneous detection of low field NMR and biomagnetic signals," *IEEE Trans. on Appl. Supercond.*, **15**, 676-679 (2005).

[5] P. Volegov, A. Matlachov, M. Espy, J. George, and R. H. Kraus Jr., "Simultaneous magnetoencephalography and SQUID detected nuclear magnetic resonance in microtesla magnetic fields," *Magn. Reson. Med.*, **52**, 467–470 (2004).

[6] V. S. Zotev et al., "Microtesla MRI of the human brain combined with MEG," *J. Magn. Reson.* , **194**, 115-120 (2008).

[7] P. Magnelind et al., "Co-Registration of Interleaved MEG and ULF MRI using a 7 channel Low-Tc SQUID system," *IEEE Trans. on Appl. Supercond.*, **21**, 456-460 (2011).

[8] M. Hämäläinen, R. Hari, R. J. Ilmoniemi, J. Knuutila, and O. V. Lounasmaa, "Magnetoencephalography - theory, instrumentation, and applications to noninvasive studies of the working human brain," *Rev. Mod. Phys.*, **65**, 413-497 (1993).

[9] IMEDCO. [Online]. http://www.imedco.ch/

[10] J. O. Nieminen et al., "Avoiding eddy-current problems in ultra-low-field MRI with self-shielded polarizing coils," *J. Magn. Res.*, **212**, 154-160 (2011).

[11] M. Packard and R. Varian, "Free nuclear induction in the Earth's magnetic field," *Phys. Rev.*, **93**, 941 (1954).

[12] S. G. Kim, "Quantification of relative cerebral blood flow change by flow-sensitive alternating inversion recovery (FAIR) technique: application to functional mapping," *Magn. Reson. Med.*, **34**, 293-301 (1995).

[13] P. Magnelind et al., Towards functional magnetic resonance imaging at ultra-low fields, 2011, Presented at the Superconductivity Centennial Conference in The Hague, The Netherlands.

[14] E. J. Woo and Seo J. K., "Magnetic resonance electrical impedance tomography (MREIT) for high-resolution conductivity imaging," *Physiol. Meas.*, **29**, R1-26 (2008).

[15] P. Mansfield, "Multi-planar image formation using NMR spin echoes," *J. Phys. C*, **10**, L55-58 (1977).

[16] J. O. Nieminen, M. Burghoff, L. Trahms, and R. Ilmoniemi, "Polarization encoding as a novel approach to MRI," *J. Magn. Reson.*, **202**, 211-216 (2010).

[17] Supracon AG. [Online]. http://www.supracon.com/

[18] E. T. Jaynes, "Matrix treatment of nuclear induction," *Phys. Rev.*, **98**, 1099-1105 (1955).

[19] W. R. Myers, "Potential Applications of Magnetic Resonance Imaging Detected Using a Superconducting Quantum Interfernce Device," UC Berkeley, Berkeley, PhD thesis 2006.

[20] R. H. Koch, J. Z. Sun, V. Foglietti, and W. J. Gallagher, "Flux dam, a method to reduce extra low frequency noise when a superconducting magnetometer is exposed to a magnetic field," *Applied Physics Letters*, **67**, 709-711 (1995).

[21] A. N. Matlashov et al., "SQUIDs vs. Induction Coils for Ultra-Low Field Nuclear Magnetic Resonance: Experimental and Simulation Comparison," *IEEE Trans. Appl. Supercond.*, **21**, 465-468 (2011).

[22] Y. Adachi et al., "A 75-ch SQUID biomagnetometer system for human cervical spinal cord evoked field," *IEEE Trans. Appl. Supercond.*, **17**, 3867-3873 (2007).

[23] M Espy et al., "Ultra-low-field MRI for the detection of liquid explosives," *Supercond. Sci. Technol.*, **23**, 034023 (2010).

[24] L.L. Tsai, R.W. Mair, M.S. Rosen, S. Patz, and R.L. Walsworth, "An Open Access, very-low-field MRI System for posture-dependent 3He Human Lung Imaging," *Journal of Magnetic Resonance*, **193**, 274-285 (2008).

[25] P. Volegov, A. Matlachov, J. Mosher, M. A. Espy, and R. H. Kraus Jr., "Noise-free magnetoencephalography recordings of brain function," *Phys. Med. Biol.*, **49**, 2117-28 (2004).